Mon. Not. R. Astron. Soc. **345,** 683–690 (2003)

The multiple stellar population in ω Centauri: spatial distribution and structural properties

E. Pancino,[1⋆] A. Seleznev,[2] F. R. Ferraro,[3] M. Bellazzini[1] and G. Piotto[4]

[1]*Osservatorio Astronomico di Bologna, via Ranzani 1, I-40127 Bologna, Italy*
[2]*Astronomical Observatory, Urals State University, Lenin's ave. 51, Ekaterinburg 620083, Russia*
[3]*Dipartimento di Astronomia, Università di Bologna, via Ranzani 1, I-40127 Bologna, Italy*
[4]*Dipartimento di Astronomia, Università di Padova, vicolo dell'Osservatorio 5, I-35122 Padova, Italy*

Accepted 2003 July 2. Received 2003 July 2; in original form 2002 December 21

ABSTRACT

We present a detailed analysis of the spatial distribution of the stellar populations in the Galactic globular cluster ω Centauri. Taking advantage of the large photometric catalogue published by Pancino et al., we confirm that metal-rich populations have a spatial distribution which is significantly different from the metal-poor dominant population. In particular (i) the different sub-populations have different centroids and (ii) the metal-poor population is elongated along the east–west direction, while the metal-rich populations are oriented along the orthogonal direction, i.e. north–south. The evidence presented here can partially explain the weird spatial metallicity segregation found by Jurcsik, and further supports the hypothesis that different subpopulations in ω Centauri might have had different origins.

Key words: globular clusters: individual: NGC 5139.

1 INTRODUCTION

The peculiar nature of the Galactic globular cluster ω Centauri has been known and studied for more than 40 years. Besides being the most massive and luminous in the Milky Way, it is presently the only globular cluster that shows a spread in its heavy elements content. Recent findings have shown that (i) at least three primary enrichment peaks do exist in this cluster, including the recently discovered metal-rich component (Lee et al. 1999; Pancino et al. 2000); (ii) an age spread of 3–5 Gyr seems to be required to explain the turn-off region morphology (Hughes & Wallerstein 2000; Hilker & Richtler 2000); (iii) the chemical enrichment of the metal-poor and intermediate stars is mainly caused by the retention of SNe II and intermediate-mass AGB star ejecta (Smith et al. 2000; Norris & Da Costa 1995); (iv) the metal-rich stars appear to have a lower α enhancement, most probably owing to SNe Ia pollution (Pancino et al. 2002).

All these pieces of evidence suggest that ω Centauri could be an intermediate object between normal globular clusters, which are unable to retain any of the supernovae ejecta, and the dwarf spheroidal galaxies (dSph), which are the smallest stellar systems capable of self-enrichment. ω Centauri could also be the remaining nucleus of a dwarf galaxy that was stripped during its interaction with the Milky Way, in possible analogy with the complex and still debated case of M54 and the Sagittarius dSph. The possibility that ω Centauri comes from 'outside' the Milky Way seems also required to explain its present orbit (Dinescu, Girard & van Altena 1999).

However, other clues complicate the picture. For example, the unusually high ellipticity of ω Cen, which has been demonstrated to be sustained by rotation (Merritt & Tremblay 1994), is compatible with the flattened shapes resulting from the merger of two globular clusters (Makino, Akiyama & Sugimoto 1991), and anyway the long relaxation time (Djorgovski 1993; Merritt, Meylan & Mayor 1997) grants that ω Centauri is not completely relaxed dynamically. Moreover, Norris et al. (1997) showed that only stars with [Fe/H] $\leqslant -1.2$ in ω Cen do rotate, while the more metal-rich components show no evident sign of rotation. Pancino et al. (2000) showed that, while the metal-poor population exhibits the well known east–west (E–W) elongation, the two metal-rich populations show a more pronounced ellipticity, but with an elongation in the north–south (N–S) direction. Finally, the most metal-rich population shows a different bulk proper motion with respect to the whole cluster (Ferraro et al. (2002b). All these results point toward a different dynamical origin for the subpopulations in ω Cen, possibly resulting from a major merger event in the cluster's past history.

Given this framework, we have started a coordinated spectrophotometric study of ω Centauri (see Pancino et al. 2000, 2002; Bellazzini, Ferraro & Pancino 2001; Ferraro, Pancino & Bellazzini 2002a; Ferraro, Bellazzini & Pancino 2002b; Origlia et al. 2003), specifically devoted to the characterization of the subpopulations, and aimed at understanding the origin and evolution of this complex stellar system. In this paper, we exploit the large number of stars (more than 230 000 in total) and the wide area coverage (33×33 arcmin^2) of the photometry published by Pancino et al. (2000),

⋆E-mail: pancino@anubi.bo.astro.it

to study in deeper detail the structural properties of the red giants in ω Centauri.

The article is organized as follows. In Section 2 we define the photometric samples corresponding to the subpopulations of giants in ω Centauri; in Section 3 we study the surface density distributions and concentration of the three subsamples; in Section 4 we measure the ellipticity, the centre positions and the orientation of the three subpopulations; in Section 5 we comment on the metallicity segregation found by Jurcsik (1998). Finally, in Section 6, we summarize our main results and discuss them in the framework of the present theories about the formation and evolution of ω Centauri.

2 SAMPLES DEFINITION

Using the metallicity information from the RGB Ca triplet survey by Norris, Freeman & Mighell (1996) and the RGB morphology from the colour–magnitude diagram, Pancino et al. (2000, see their fig. 2) identified three subpopulations of RGB stars, with different average metallicity and photometric properties. To analyse in detail the structural properties of these subpopulations, we have extracted from the Pancino et al. (2000) catalogue the following photometric samples (with $B < 16$ mag).

(i) The RGB-MP sample, corresponding to the main, metal-poor peak of the metallicity distribution, around [Ca/H] ~ -1.4 or [Fe/H] ~ -1.7. This population comprises $\sim$70 per cent of the whole RGB population, and our photometric sample contains 2630 stars.

(ii) The RGB-MInt sample, comprising the secondary, intermediate metallicity peak around [Ca/H] ~ -1.0 or [Fe/H] ~ -1.2, together with the long, extended tail to higher metallicities. This subpopulation accounts for $\sim$25 per cent of the whole RGB population, and our sample contains 816 stars.

(iii) The RGB-a sample, the newly discovered metal-rich population that comprises $\sim$5 per cent of the RGB stars and has a metallicity of [Ca/H] ~ -0.5 and [Fe/H] ~ -0.6 (Pancino et al. 2002). Our photometric sample contains 128 stars. Although this last subpopulation has many fewer stars, it is the most numerous sample presently at our disposal, and its size could be significantly increased only when the RGB-a counterparts in other evolutionary phases (i.e. horizontal branch, subgiant brach and main sequence) are identified.

3 SURFACE DENSITY DISTRIBUTIONS

We computed the surface density distributions of the three subpopulations defined in Section 2, using a fixed kernel estimator algorithm (Silverman 1986; Merritt & Tremblay 1994; Seleznev 1998), with a kernel half-width of 500 pixel[1] and a grid of 100 pixel cells. The resulting surface density plots are shown in Fig. 1, where the isodensity contour lines shown are normalized to the maximum density of each distribution, in steps of 10 per cent. From now on, we will refer to each isodensity level using the fraction of the peak value, i.e. 0.3 for the isodensity level corresponding to 30 per cent of the peak value. The peak density values are: 48.3 star arcmin^{-2} for the RGB-MP sample, 14.6 star arcmin^{-2} for the RGB-MInt sample and 2.3 star arcmin^{-2} for the RGB-a sample.

A first, qualitative comparison of the three distributions shown in Fig. 1 reveals the following general facts.

[1] In what follows, it is useful to bear in mind that the WFI scale is 0.238 arcsec pixel^{-1}. Thus, 100 pixel corresponds approximately to 24 arcsec.

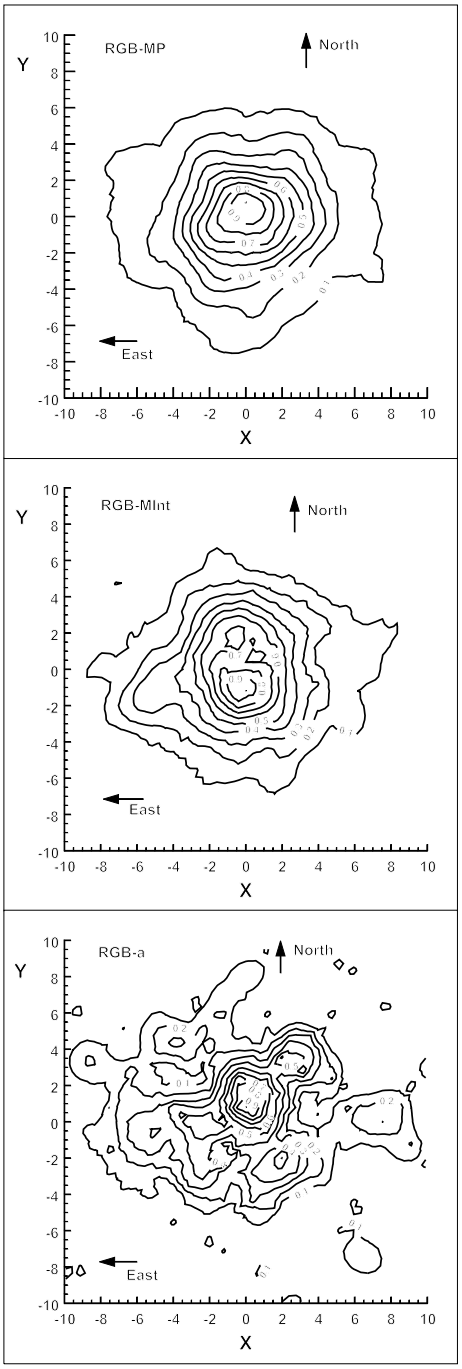

Figure 1. Isodensity contour lines for the three RGB samples defined in the text: the RGB-MP (upper panel), the RGB-MInt (middle panel) and the RGB-a (lower panel). The contour lines are normalized to their peak density and are plotted in steps of 10 per cent of the peak density. In all panels the axes show the distance from the cluster centre (700 $\pm$ 20 pixel, 1900 $\pm$ 20 pixel), in arcmin.

(i) The RGB-MP population is clearly elongated along the E–W direction, reflecting the well-known elliptical shape of the whole system. The main peak position is consistent with the cluster centroid estimated by Pancino et al. (2000).

(ii) Both the RGB-a and the RGB-MInt populations have perturbed isodensity contour lines, showing structures similar to bubbles, shells and/or tails. While in the case of the RGB-a sample the

Table 1. Results of the two-dimensional generalization of the K–S test for the three subpopulations. The first column shows the populations that are actually compared, the second shows the maximum difference in the cumulative distributions D, while the third column shows the derived probability P that the two populations are drawn from the same parent distribution.

Population	D	P
RGB-a vs. RGB-MP	0.171	0.012
RGB-MInt vs. RGB-MP	0.068	0.039
RGB-MInt vs. RGB-a	0.117	0.225

Table 2. For each subpopulation (column 1), the equivalent radius, in pixels, of the ellipses used to approximate the 90 per cent isodensity contour lines (close to the peak) is shown in column 2 ($r_{e,90\,\mathrm{per\,cent}}$) and its ratio with the radius of the RGB-MP population in column 3 ($R_{90\,\mathrm{per\,cent}}$). Columns 4 and 5 show the corresponding values ($r_{e,60\,\mathrm{per\,cent}}$ and $R_{60\,\mathrm{per\,cent}}$) for the ellipses used to approximate the 60 per cent isodensity contour level (close to half maximum).

Population	$r_{e,90\,\mathrm{per\,cent}}$	$R_{90\,\mathrm{per\,cent}}$	$r_{e,60\,\mathrm{per\,cent}}$	$R_{60\,\mathrm{per\,cent}}$
RGB-MP	213.8 ± 6.5	1.00	578.9 ± 13.5	1.00
RGB-MInt	169.3 ± 15.9	0.79	601.7 ± 7.6	1.04
RGB-a	66.2 ± 5.5	0.31	323.1 ± 5.0	0.56

complexity increases in the outer parts, where it is almost certainly caused by low number statistics, in the case of RGB-MInt we find complex structures in the central parts, where data points are more numerous.[2]

(iii) The RGB-MInt population is clearly elongated along the N–S direction in the inner parts, while in the external parts it seems to become elongated in the E–W direction. The main peak lies south of the RGB-MP peak, with a possible secondary peak north of it, which gives an evident asymmetric shape to the distribution.

(iv) The RGB-a population is also elongated along the N–S direction in its inner parts; its main peak lies north of the RGB-MP peak.

A simple monodimensional Kolmogorov–Smirnov test (K–S, see e.g. Press et al. 1997) as a function of a radial coordinate is not sufficient to assess properly the significance of these features. We thus used a two-dimensional generalization of the K–S statistical test, which was proposed and investigated with Monte Carlo experiments by Fasano & Franceschini (1987), as a variant of an earlier idea by Peacock (1983). This test, similarly to the usual K–S test, quantifies the probability P that two (two-dimensional) distributions are extracted from the same parent distribution, using a more sophisticated definition of the maximum difference D in the cumulative distributions.

The results are summarized in Table 1. The very low probabilities obtained in the comparison of the RGB-MP population with both the RGB-MInt and the RGB-a ensures us that their spatial distributions are significantly different, i.e. they cannot be drawn from the same parent distribution. On the other hand, the probability obtained in the comparison between the RGB-MInt and the RGB-a populations confirms that they are not significantly different from each other.

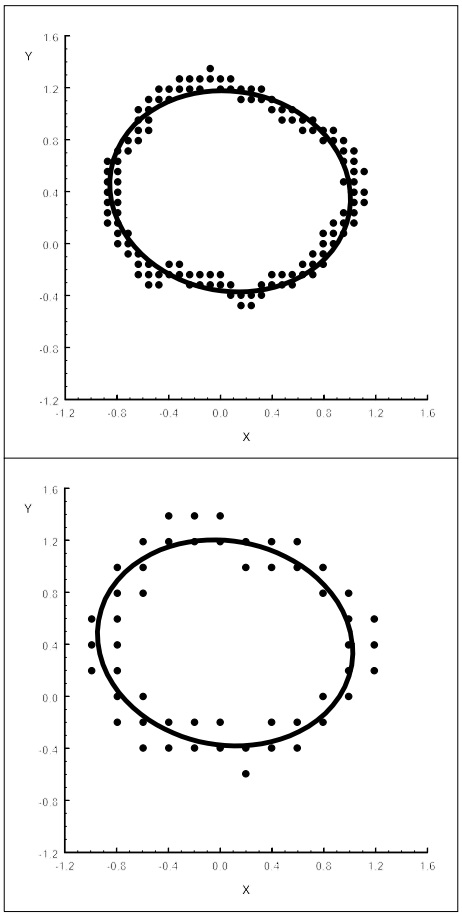

Figure 2. Example of the approximation of the 0.9 isodensity contour line with an ellipse, for the RGB-MP. Top panel: the black dots represent the points in the 20-pixel grid that are closer to 90 per cent of the peak value; the solid ellipse is the best fit. Bottom panel: same as above, but this time with the 50-pixel grid: the final best-fitting ellipse is slightly different.

We can also notice from Fig. 1 that the RGB-a population appears *more* concentrated than the RGB-MP one, while we cannot say much about the RGB-MInt population, which has a complicated shape in its inner isodensity contour lines. A more quantitative evaluation confirms this impression: Table 2 reports the equivalent radii[3] of the three subpopulations, calculated with the ellipse parameters derived in Section 4, for the 0.9 and 0.6 isodensity contour lines. The RGB-a equivalent radii are ∼2–3 times smaller than the RGB-MP correspondent radii.

4 ELLIPTICITY

To describe in a more quantitative way the shape and structure of the subpopulations defined in Section 2, we fitted ellipses to the isodensity contours of each sample. The spatial distributions were derived as in Section 3, with the same kernel, but using higher resolution grids of 20 and 50 pixel cells. We used the finer grid (20 pixel) for the internal regions that are more densely populated, i.e. within the 0.6 isodensity level, and the coarser grid (50 pixel)

[2] We would like to recall here that, as recently reviewed by Lub (2002), differential reddening is not significant in ω Cen. In fact, Cannon (1980) showed that no nebulosity or patchy obscuration is present in front of the cluster. This result is confirmed by large-scale reddening maps (Burstein & Heiles 1982; Schlegel, Finkbeiner & Davis 1998). Also, the absence of dense interstellar medium within ω Cen has been proven with an ISOCAM study by Origlia et al. (2003). Thus, the observed structures cannot be due to differential reddening.

[3] The equivalent radius for an ellipse of semi-axes a and b is defined as $r_e = \sqrt{ab}$, i.e. the radius of a circle with the same area.

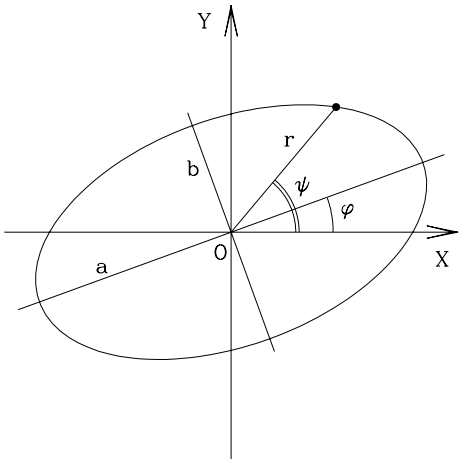

Figure 3. Ellipse parameters notation: O is the ellipse centre; X and Y are the axes of the usual Cartesian reference frame, while ψ and r are the angular and radial coordinates in the polar coordinate system; a and b are the ellipse semimajor and semiminor axes, respectively; φ is the major axis inclination with respect to the X axis.

for the outer regions. As in Section 3, we defined densities in units of maximum (peak) density for each distribution, and we chose isodensity levels going from 90 per cent to 10 per cent of the peak density, in steps of 10 per cent. Ellipses were fitted to each isodensity line, defined by those grid nodes that bracket the chosen density value (see Fig. 2). The best-fitting ellipses are hereafter designated with the same notation used for the isodensity contours in Fig. 1, i.e. 0.9 for the 90 per cent ellipse and so on.

Kholopov (1953) suggested that the best way to approximate equal density lines with ellipses in globular clusters is to use polar coordinates (r, ψ). This method has the advantage that the deviations of points from the ellipse along the radial direction are close to the deviations in the direction perpendicular to the ellipse. In polar coordinates, the ellipses have the following form:

$$\frac{1}{r^2} = A + B \sin 2\psi + C \cos 2\psi. \quad (1)$$

The relations of the coefficients A, B and C with the usual ellipse parameters (Fig. 3) are

$$A = \frac{1}{2}\left(\frac{1}{a^2} + \frac{1}{b^2}\right),$$

$$B = \frac{1}{2}\left(\frac{1}{a^2} - \frac{1}{b^2}\right) \sin 2\varphi,$$

$$C = \frac{1}{2}\left(\frac{1}{a^2} - \frac{1}{b^2}\right) \cos 2\varphi.$$

As demonstrated by earlier studies (Geyer, Nelles & Hopp 1983), the a priori adoption of the cluster centre position can produce errors (i.e. an overestimation) on the ellipticity estimate. This point is even more important in our particular case, since we suspect that the centroids of the three subpopulations differ from each other. Therefore, we determined the coordinates of each ellipse centre as the mean coordinates of the input points on each isodensity line. The ellipse coefficients A, B and C where determined by least square approximation with singular value decomposition (Press et al. 1997). An example of the result of the fitting procedure is shown in Fig. 2.

Table 3. The density peaks of the whole RGB sample and of the three subsamples (in pixels), represented by the centres of the 80 per cent isodensity level fits. The distance of each population from the RGB total sample is calculated, both in pixels and in arcsec. The last row reports the corresponding distance between the present RGB global sample and the cluster centroid determined by Pancino et al. (2000).

Population	X_C (pixel)	Y_C (pixel)	d (pixel)	d ($''$)
RGB-tot	689 ± 8	1906 ± 12	–	–
RGB-MP	701 ± 9	1954 ± 17	49 ± 24	12 ± 6
RGB-MInt	651 ± 10	1671 ± 16	238 ± 24	57 ± 6
RGB-a	761 ± 9	2194 ± 8	297 ± 19	71 ± 5
ω Centauri	700 ± 20	1900 ± 20	12 ± 32	3 ± 8

4.1 Ellipse centres

Following the procedure described above, we determined the ellipse centres for each of the three subpopulations defined in Section 2, and for each isodensity level. The same procedure has been applied, for ease of comparison, also to the total RGB sample, defined as the union of the three subsamples. The results are listed in Table 3: the RGB-MInt and RGB-a centres are significantly different from the RGB-MP centre. We can also compare with the centre position found by Pancino et al. (2000), which is $(700 \pm 20, 1900 \pm 20)$ in the WFI pixel system. As we can see, the centre of the global RGB sample is perfectly compatible with that estimate.

A look at the centre position trend with the isodensity level (Fig. 4) shows that the RGB-MP, dominating the cluster population, has a quite stable centre position and coincides reasonably well with the

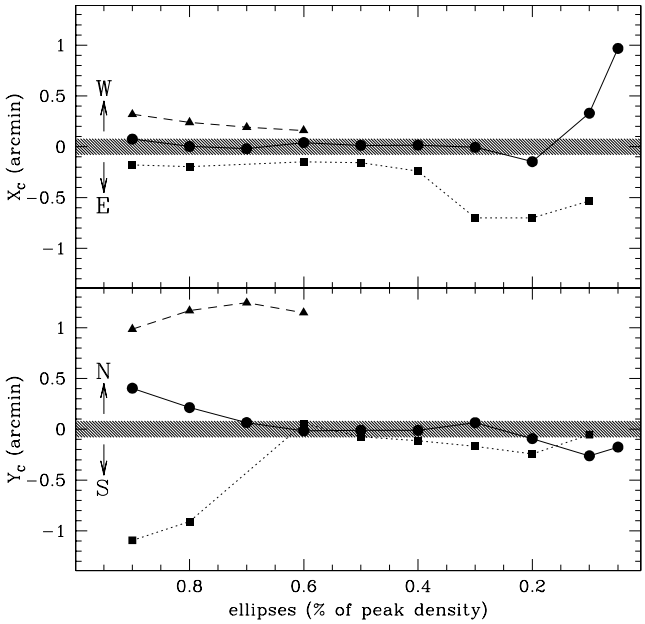

Figure 4. Displacement of the ellipse centres for the three subpopulations. Ellipses are denominated along the abscissae in fractions of the peak value, as described in the text. The shaded area represents the cluster centre position determined by Pancino et al. (2000), ($X_C = 700 \pm 20$ pixel, $Y_C = 1900 \pm 20$ pixel). The three subpopulations are marked with different symbols: *filled dots* for the RGB-MP, *filled squares* for the RGB-MInt and *filled triangles* for the RGB-a. The *top panel* shows the displacements in the E–W direction, i.e. along the X CCD axis, while the *bottom panel* shows the displacements along the N–S direction, i.e. the Y CCD axis. The error bars are smaller than the symbols.

centre of ω Centauri measured by Pancino et al. (2000), except for its two inner isodensity levels. The RGB-MInt centre is slightly displaced to the east ($\sim$10 arcsec) and significantly to the south ($\sim$1 arcmin), at least for the inner fits. This reflects the behaviour seen in Fig. 1: in the central parts the main peak of the population is clearly S–E of the RGB-MP population, while the behaviour in the external parts becomes smoother. The RGB-a centre is instead slightly displaced to the west ($\sim$10 arcsec), and significantly to the north ($\sim$1 arcmin), at least for the few isodensity contour lines that we were able to fit with ellipses. Again, this reflects what seen in Fig. 1. We recall here that the literature estimates of ω Centauri's core radius go from a maximum of $r_c = 2.89$ arcmin (Trager, King & Djorgovski 1995) to a minimum of $r_c = 1.4$ arcmin (van Leeuwen et al. 2000), so the observed displacements are comparable in size to the core radius of ω Centauri.

4.2 Flattening and orientation

As shown in Table 4, the three subpopulations axial ratios have similar behaviours, within the error bars. They do not show dramatic trends moving away from the centre, with both the RGB-MP and the RGB-MInt becoming slowly rounder away from their density peaks. For the RGB-a, owing to the low number of objects in the external parts, only the inner isodensity levels could be fitted. The weighted averages of the axial ratios shown in Table 4 are: $\langle(b/a)\rangle = 0.81 \pm 0.01$ for the RGB-MP, $\langle(b/a)\rangle = 0.81 \pm 0.06$ for the RGB-MInt and $\langle(b/a)\rangle = 0.78 \pm 0.11$ for the RGB-a.

Table 4. Axial ratio and orientation for the best-fit ellipses for the whole RGB sample and for each subsample. Each best-fitting ellipse is designated with the fraction of the peak density for each population, as described in the text. The axial ratio (b/a) and the inclination angle φ (i.e. the angle in degrees, counted from west to north) are also shown.

Population	Grid	Ellipse	$(b/a) \pm \delta(b/a)$	$\varphi \pm \delta\varphi$
RGB-tot	20	0.9	0.92 ± 0.01	49.2 ± 5.7
	20	0.8	0.93 ± 0.01	26.3 ± 4.9
	20	0.7	0.93 ± 0.02	17.5 ± 3.5
	20	0.6	0.93 ± 0.01	19.5 ± 2.9
	50	0.5	0.93 ± 0.02	18.0 ± 4.3
	50	0.4	0.93 ± 0.02	20.9 ± 4.7
	50	0.3	0.92 ± 0.02	31.9 ± 3.3
	50	0.2	0.89 ± 0.01	32.0 ± 2.7
	50	0.1	0.84 ± 0.01	3.7 ± 1.7
	50	0.05	0.84 ± 0.03	6.0 ± 1.2
RGB-MP	20	0.9	0.82 ± 0.05	-10.4 ± 3.1
	20	0.8	0.80 ± 0.12	3.8 ± 2.4
	20	0.7	0.79 ± 0.05	7.0 ± 1.7
	20	0.6	0.81 ± 0.04	7.0 ± 1.4
	50	0.5	0.84 ± 0.03	12.4 ± 2.6
	50	0.4	0.85 ± 0.02	15.8 ± 2.7
	50	0.3	0.88 ± 0.02	22.7 ± 3.2
	50	0.2	0.90 ± 0.01	41.9 ± 2.8
	50	0.1	0.85 ± 0.04	8.6 ± 2.2
	50	0.05	0.85 ± 0.02	10.9 ± 1.6
RGB-MInt	20	0.9	0.85 ± 0.16	-8.0 ± 8.9
	20	0.8	0.73 ± 0.10	-6.1 ± 2.4
	20	0.6	0.75 ± 0.02	100.2 ± 0.8
	50	0.5	0.77 ± 0.03	100.8 ± 1.6
	50	0.4	0.87 ± 0.03	102.2 ± 2.8
	50	0.3	0.90 ± 0.02	33.0 ± 6.4
	50	0.2	0.88 ± 0.02	24.3 ± 3.8
	50	0.1	0.83 ± 0.06	6.3 ± 2.2
RGB-a	20	0.9	0.66 ± 0.11	47.2 ± 10.7
	20	0.8	0.86 ± 0.12	97.9 ± 7.2
	20	0.7	0.81 ± 0.04	112.7 ± 4.7
	20	0.6	0.83 ± 0.03	108.7 ± 2.9

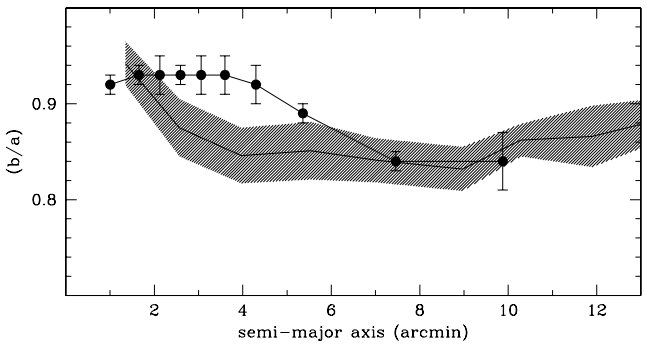

Figure 5. Axial ratio for the whole RGB population (black dots; see also Table 4), compared with the measurements by Geyer et al. (1983; see their table 4), represented by the shaded area.

To compare our results with previous work, we performed the same measurements on the entire RGB sample, resulting from the union of the three subsamples defined in Section 2. In particular, Fig. 5 shows the comparison with Geyer et al. (1983, see their table 4): the overall agreement is reasonably good, with a marginal discrepancy in the region between 2.′5 and 4.5 arcmin from the cluster centre. Moreover, our average axial ratio and ellipticity ($\varepsilon = 1 - b/a$) for the whole RGB sample, $\langle(b/a)\rangle = 0.89 \pm 0.04$ and $\langle\varepsilon\rangle = 0.11 \pm 0.04$, compare well with previous results like $\langle(b/a)\rangle = 0.83 \pm 0.03$ (White & Shawl 1987), $\langle\varepsilon\rangle = 0.12 \pm 0.04$ (Geyer et al. 1983) or $\langle\varepsilon\rangle = 0.077$ (van Leeuwen et al. 2000).

Finally, while the flattenings of the three subpopulations appear rather similar, the orientations of the best-fitting ellipses are instead quite different (see Table 4). The RGB-MP major axis is always close to the E–W direction, with $\langle\varphi\rangle \sim -4^\circ \pm 10^\circ$, and its inclination seems to increase slowly with the distance from the cluster centre, although at these low flattenings the uncertainty on the inclination angle can be substantially higher than the formal errors quoted in Table 4 (Geyer et al. 1983). The RGB-MInt shows instead a complex structure in the central parts (Fig. 1), with a possible double peak. But its 0.6–0.4 isodensity levels (the most reliable ones) are always inclined along the N–S direction, with $\langle\varphi\rangle \sim 100^\circ$, while the outer parts suddenly drop to $\langle\varphi\rangle \sim 25^\circ$, much closer to the E–W direction. Finally, the RGB-a is oriented along the N–S direction, although ellipses could be fitted only to the inner parts, with $\langle\varphi\rangle$ close to 90°–100°, except for the innermost fit. Again, these quantitative estimates closely reflect what is seen in Fig. 1.

5 METALLICITY SEGREGATION

Recently Jurcsik (1998), using a compilation of good-quality spectroscopic data from the literature, has shown that the bright giants ($V \leqslant 12.75$) in ω Centauri, belonging to the two metallicity groups with [Fe/H] $\leqslant -1.75$ and [Fe/H] $\geqslant -1.25$, have a weird spatial distribution. Each of the two groups occupies one half of the cluster: no star of one group is found on the other side and the two centroids are separated by 6.2 arcmin (see her fig. 1). The separation line runs approximately perpendicular to the apparent minor axis of the cluster, which is roughly oriented towards the Galactic centre: the most metal-rich giants are on the southern half, which faces the Galaxy.

Ikuta & Arimoto (2000) questioned this effect. They used the same compilation of data and showed that no spatial segregation of stars with different metallicity is evident. However, we would

like to note here that, as clearly stated by Jurcsik (1998), the effect is only visible if one applies the specified selections, i.e. *only for bright stars of the two extreme metallicity groups*. The effect was instead partially confirmed by Hilker & Richtler (2000), who measured abundances of stars in ω Centauri with Strömgren metallicity indexes. Their fig. 15 shows a clear segregation of the most metal-rich stars in the southern half of the cluster, but they could not confirm the segregation of the most metal-poor stars.

The metal-rich group in Jurcsik (1998), with [Fe/H] $\geqslant -1.25$, is mainly a subsample of our RGB-MInt population, which has a pronounced peak just $\sim$1 arcmin south of the cluster centre (see Fig. 1 and Table 3), a value that is roughly compatible with the Jurcsik estimate ($\sim$3 arcmin). We thus easily explain the observed segregation of her metal-rich group, since when one draws randomly a sample of metal-rich stars, there is a higher probability to find them close to the main peak of the density distribution, i.e. in the southern half of the cluster.

Jurcsik (1998) metal-poor group, with [Fe/H] $\leqslant -1.75$, is instead a subsample of our RGB-MP, or more precisely it represents the lowest metallicity tail of the RGB-MP. We tried to isolate this subpopulation by dividing our RGB-MP sample, in the $(I, B-I)$ plane into three strip-like subsamples, equally wide in colour: (i) the bluest RGB-MP subsample, the RGB-MP1, most probably corresponding to Jurcsik's metal-poor group; (ii) the intermediate subsample, the RGB-MP2 and (iii) the reddest subsample, the RGB-MP3. A two-dimensional KS test, like the one described in section 3, gives a low probability that the RGB-MP1 is extracted from the same parent distribution of the RGB-MP2 ($P_{12} = 1.4210^{-6}$) or RGB-MP3 ($P_{13} = 3.9210^{-5}$). However, we were not able to measure any significant difference in the peaks positions or in the concentration of the RGB-MP subsamples.

We thus are unable to explain the metal-poor part of the spatial metallicity segregation found by Jurcsik (1998) on the basis of our photometric catalogue. If the Jurcsik (1998) effect will be confirmed and understood in the future, it could mean that an additional, metal-poor subpopulation exists in ω Centauri, with its own distinct properties. Otherwise, the observed spatial segregation of that group of stars could simply be the result of a statistical fluctuation, explaining why Hilker & Richtler (2000) were not able to confirm the metal-poor part of the segregation effect. More data on abundances of a significant sample of stars with [Fe/H] $\leqslant -1.75$ are thus needed to explain completely this second half of the puzzle.

6 SUMMARY AND DISCUSSION

Using the nomenclature defined in Pancino et al. (2000), we have selected three samples with $B < 16$: the RGB-MP, the RGB-MInt and the RGB-a. We have shown that the three samples are significantly different in their spatial and structural properties, in particular in the respects listed below.

(i) Both the RGB-MInt and the RGB-a main density peaks are shifted by $\sim$1 arcmin with respect to the cluster centre.

(ii) Both the RGB-a and the RGB-MInt populations are elongated on a direction that is perpendicular to the elongation of the RGB-MP population.

(iii) The RGB-a population is significantly more concentrated than the RGB-MP population. No firm conclusion can be reached for the RGB-MInt, owing to the complex isodensity contour line's shapes in its central parts.

(iv) Both the RGB-MInt and the RGB-a show complex and perturbed isodensity contour lines, resembling bubbles, shells and tails. While for the outer isodensity contours this can be caused by statistical undersampling (especially for the RGB-a), in the inner parts these features are probably real.

(v) Finally, we were able to explain the metal-rich part of the weird spatial metallicity segregation, found by Jurcsik (1998) and confirmed by Hilker & Richtler (2000), thanks to the peculiar surface density distribution of the RGB-MInt and, in particular, to its centre displacement with respect to the RGB-MP centre.

Let us discuss these findings in the framework of the current scenarios for the formation and evolution of ω Centauri. As briefly mentioned in Section 1, there is a consistent body of evidence supporting the fact that ω Centauri built up by itself at least part of the chemical elements that we can observe today. In a standard self-enrichment scenario, we would expect the more metal-rich (and younger) populations to be more centrally concentrated than the metal-poor, dominant population. This is almost always the case for the dwarf galaxies of the local group, with only a few exceptions (Harbeck et al. 2001), and it is exactly what we observe for ω Centauri (point (iii) above).

Unfortunately, while there is no doubt on the fact that self-enrichment must be one of the fundamental ingredients of a successful formation and evolution theory for ω Centauri (Norris & Da Costa 1995; Smith et al. 2000), we are dealing with a complex set of observational facts, containing conflicting evidence. In fact, a few of the observational properties of ω Centauri, concerning the structure, the shape and the kinematics (Section 1) are not easily accommodated into a simple self-enrichment scenario (Norris et al. 1997; Pancino et al. 2000; Ferraro et al. 2002b), and suggest the possibility of a merger or accretion event. However, the simple merging of two or more single-metallicity clusters cannot account for the broad metallicity distribution of the RGB (Norris et al. 1996; Smith et al. 2000) and the high speed of ordinary, already formed globular clusters in the present potential well of the Milky Way makes this kind of merging quite unlikely (Thurl & Johnston 2002).[4] The evidence presented here, concerning the structure and shape of the different subpopulations in the RGB of ω Centauri, supports these findings and thus confirms the need for a more sophisticated scenario that takes into account *all* the observational evidence collected so far.

6.1 A complex dynamical history

Let us first discuss the relative orientation of the three RGB subpopulations. It is now well established that the elongated shape of the whole cluster (dominated by the RGB-MP population) is mainly the result of rotation (Harding 1965; Merritt & Tremblay 1994; Meylan & Mayor 1986), which is consistent with the picture of a dynamically young and not completely relaxed cluster: the cluster's peak rotational velocity is 7 km s^{-1} at 11 pc from the centre (Merritt et al. 1997) and the relaxation times for ω Centauri are of the order of magnitude of its age, being $\log t_{\rm rc} = 9.73$ yr in the core and $\log t_{\rm rh} =$ 10 yr at half mass (Harris 1996).

Thus, it becomes tempting to explain the elongations of the RGB-MInt and RGB-a populations in terms of rotational velocity, too, but in this case it would be necessary to assume that these two populations rotate around a *perpendicular axis* with respect to the

[4] Of course, in a lower potetial environment like the Fornax dwarf spheroidal, the chance would be substantially higher. Moreover, mergers between protocluster clouds have been very recently explored by Tsujimoto & Shigeyama (2003), in the context of an inhomogeneous chemical evolution model, as a possible mechanism of formation of normal GGC. This secnario would also naturally explain the formation of rare objects like ω Cen.

RGB-MP. An inspiring comparison is posed by the recent work by Sarzi et al. (2000), who examine an example of galaxy that has undergone a major merging or accretion event in its past. The signature of such an event is the simultaneous presence of (1) an orthogonally elongated bulge with respect to the disc, and of (2) two rotation curves, perpendicular to each other, one for the host galaxy and another for the accreted component.

Now, we have shown here (point ii above) that the first signature could indeed be present in ω Centauri: we have (at least) two components with orthogonal elongations. What can we say about the rotation curves? It has been demonstrated in the past (Norris et al. 1997) that while the metal-poor stars in ω Centauri rotate, no sign of rotation is evident for the metal-rich stars. Again, the metal-rich stars of Norris correspond mainly to our RGB-MInt population, while too few data are presently available for the RGB-a population. So, the second signature is only partially present in ω Centauri. Clearly, to demonstrate or falsify the point fully, one needs more precise radial velocities for a much larger sample of RGB-MInt and RGB-a stars, and a model which is best suited to small systems embedded in a common potential well. For example, if we consider simulations of the merger of two globular clusters with unequal masses (Makino et al. 1991), the most massive object retains a larger share of the initial orbital angular momentum, as Norris et al. (1997) point out to explain why we see rotation for the metal-poor stars and not for the metal-rich ones.

6.2 An accreted component?

Another interesting point has recently emerged from the coupling of the photometric catalog by Pancino et al. (2000) and the proper motion work by van Leeuwen et al. (2000), i.e. that the RGB-a population appears to have a different bulk proper motion of $|\delta\mu| = 0.8$ mas yr^{-1} with respect to the main population of ω Centauri (Ferraro et al. 2002b). This evidence suggests that the RGB-a could be an accreted population, captured by the main body of ω Centauri. We thus should expect the RGB-a to have a different centre from the main cluster population, too, and it is exactly what we find here [point (i) above]. Moreover, if a merging event has really taken place in the past history of ω Centauri, how long ago do we expect it to have happened? We already know that ω Centauri has a very long relaxation time, comparable to its age. We also know that the RGB-a is $\sim$2–3 times more concentrated than the RGB-MP (point (iii) above), and the fact that it is almost one core radius away from the centre suggests that it is moving in a significantly less dense environment, so it could have survived as a self-gravitating system for many Gyr. It is however puzzling that the (few) radial velocities measured for the RGB-a so far are not so different from the cluster average.[5]

So, a self-consistent set of observational facts, supporting the occurrence of an accretion or merger event in the cluster past history, is beginning to take shape. We would like to note here that this fact in not necessarily in contradiction with the occurring of self-enrichment, nor with the hypothesis that ω Centauri is the remaining nucleus of a larger body (a dwarf galaxy), accreted and partially disrupted by the Milky Way. If we consider the case of the Sagittarius dwarf spheroidal (Sgr), which is the only one showing some resemblance with the case of ω Centauri, we see that more than one GC seems to be associated with the system. In particular, one of these (Terzan 7) has a metallicity of [Fe/H] ~ -0.62 (Harris 1996) compared with the [Fe/H] ~ -1.59 of M54, which may be the nucleus of the Sgr. Interestingly, the RGB-MP has a similar metallicity to that of M54, and the RGB-a to Terzan 7.[6]

6.3 A promising framework

An interesting scenario, that could accommodate all of the observational evidence collected so far, was discussed by, e.g., Freeman (1985), Norris et al. (1997) and Smith et al. (2000): the so-called *merger within a fragment scenario*, descending from the general framework proposed by Searle (1977) and Searle & Zinn (1978). In this framework, a conglomerate of star-forming subsystems or regions could evolve within a large cloud and a common potential well (a fragment), each section evolving with slightly different time-scales, and slightly different chemical properties. In this context, the chemical evolution of the RGB-MP and of the RGB-MInt could have been tightly related to each other, especially since there are reasons to believe that the RGB-MInt is younger by a few Gyr (Hughes & Wallerstein 2000) and could have been enriched by the ejecta of the RGB-MP stars.

Later, a dwarf galaxy with its own globular cluster system could form, and a few globular clusters (like the RGB-a, or even the RGB-MInt) could spiral towards the system centre, while the remaining clusters could be stripped by the interaction with the Milky Way, along with most of the dwarf galaxy halo. Recent calculations by Bromm & Clarke (2002) support this line of reasoning (see also Fellhauer & Kroupa 2002), together with the example of the Sagittarius dwarf galaxy discussed above.

Although still speculative, this idea deserves to be further explored since it appears the most promising to explain ω Centauri's puzzling properties.

ACKNOWLEDGMENTS

We thank E. Pignatelli and E. Pompei for interesting discussions on galaxy mergers. The financial support of the *Agenzia Spaziale Italiana* (ASI) is kindly acknowleged. This research was also partially supported by the Italian *Ministero dell'Istruzione dell'Universitè e della Ricerca* (MIUR). E. Pancino is grateful to the European Southern Observatory (ESO), where part of this work was carried out, within the *Studentship Programme*. A. Seleznev acknowledges the support of the Russian Federation State Scientific and Technical Program *'Astronomy'*. This paper was based on Wide Field Image data collected at the European Southern Observatory, La Silla, Chile during the observing programmes 62.L-0354 and 63.L-0439.

REFERENCES

Bellazzini M., Ferraro F. R., Pancino E., 2001, MNRAS, 327, L15
Bromm V., Clarke C. J., 2002, ApJ, 566, L1
Dinescu D. I., Girard T. M., van Altena W. F., 1999, AJ, 117, 1792
Djorgovski S., 1993, ASP Conf. Ser. Vol. 50, Structure and Dynamics of Globular Clusters. Astron. Soc. Pac., San Francisco, p. 373
Fasano G., Franceschini A., 1987, MNRAS, 225, 155
Fellhauer M., Kroupa P., 2002, Ap&SS, 281, 355
Ferraro F. R., Pancino E., Bellazzini M., 2002a, ASP Conf. Ser. Vol. 265, Omega Centauri, A Unique Window into Astrophysics. Astron. Soc. Pac., San Francisco, p. 407

[5] In this respect, it should be noted that we could be seeing the RGB-a 'orbit' from its pole, although this configuration does not have a large probability of being observed.

[6] An interesting discussion on the survival of globular clusters within dwarf elliptical galaxies has been presented by Lotz et al. (2001).

Ferraro F. R., Bellazzini M., Pancino E., 2002b, ApJ, 573, L95
Freeman K. C., 1985, IAU Symp. 113, Dynamics of Star Clusters. Astron. Soc. Pac., San Francisco, p. 33
Geyer E. H., Nelles B., Hopp U., 1983, A&A, 125, 359
Harbeck D. et al., 2001, AJ, 122, 3092
Harding G. A., 1965, Royal Greenwich Observatory Bulletin, 99, 65
Harris W. E., 1996, AJ, 112, 1487
Hilker M., Richtler T., 2000, A&A, 362, 895
Hughes J., Wallerstein G., 2000, AJ, 119, 1225
Ikuta C., Arimoto N., 2000, A&A, 358, 535
Jurcsik J., 1998, ApJ, 506, L113
Kholopov P. N., 1953, Publ. Astron. Sterneberg Inst., 23, 250
Lee Y. W., Joo J. M., Sohn Y. J., Rey S. C., Lee H. C., Walker A. R., 1999, Nat, 402, 55
Lotz J. M., Telford R., Ferguson H. C., Miller B. W., Stiavelli M., Mack J., 2001, ApJ, 552, 572
Makino J., Akiyama K., Sugimoto D., 1991, Ap&SS, 185, 63
Merritt D., Tremblay D., 1994, AJ, 108, 514
Merritt D., Meylan G., Mayor M., 1997, AJ, 114, 1074
Meylan G., Mayor M., 1986, A&A, 166, 122
Norris J. E., Da Costa G. S., 1995, ApJ, 447, 680
Norris J. E., Freeman K. C., Mighell K. L., 1996, ApJ, 462, 241
Norris J. E., Freeman K. C., Mayor M., Seitzer P., 1997, ApJ, 487, L187
Origlia L., Ferraro F. R., Bellazzini M., Pancino E., 2003, ApJ, 591, 916
Pancino E., Ferraro F. R., Bellazzini M., Piotto G., Zoccali M., 2000, ApJ, 534, L83
Pancino E., Pasquini L., Hill V., Ferraro F. R., Bellazzini M., 2002, ApJ, 568, L101
Peacock J. A., 1983, MNRAS, 202, 615
Press W. H., Teukolsky S. A., Vetterling W. T., Flannery B. P., 1997, Numerical Recipes of Fortran 77. The art of Scientific Computing, 2nd edn. Cambridge Univ. Press, New York
Sarzi M., Corsini E. M., Pizzella A., Vega Beltrán J. C., Cappellari M., Funes J. G., Bertola F., 2000, A&A, 360, 439
Searle L., 1977, in Tinsley B. M., Larson R. B., eds, The Evolution of Galaxies and Stellar Populations. Yale Univ. Obser., New Haven, p. 219
Searle L., Zinn R., 1978, ApJ, 225, 357
Seleznev A. F, 1998, Astron. Rep., 42, 153
Silverman B. W., 1986, Monographs on Statistics and Applied Probability. Chapman and Hall, London
Smith V. V., Suntzeff N., Cunha K., Gallino R., Busso M., Lambert D., Straniero O., 2000, AJ, 119, 1239
Thurl C., Johnston K. V., 2002, ASP Conf. Ser. Vol. 265, Omega Centauri, A Unique Window into Astrophysics. Astron. Soc. Pac., San Francisco, p. 337
Trager S. C., King I. R., Djorgovski S., 1995, AJ, 109, 218
van Leeuwen F., Le Poole R. S., Reijns R. A., Freeman K. C., de Zeeuw P. T., 2000, A&A, 360, 472
White R. E., Shawl S. J., 1987, ApJ, 317, 246

This paper has been typeset from a TEX/LATEX file prepared by the author.